VISUALIZING AND QUANTIFYING THE RESIDUAL PHASE DISTRIBUTION IN CORE MATERIAL

Munish Kumar, Tim J. Senden, Adrian P. Sheppard,
Jill P. Middleton & Mark A. Knackstedt
Department of Applied Mathematics, Australian National University, Canberra, Australia

This paper was prepared for presentation at the International Symposium of the Society of Core Analysts held in Noordwijk, The Netherlands 27-30 September, 2009

ABSTRACT

At the conclusion of flooding in an oil- or gas-bearing reservoir, a significant fraction of the original hydrocarbon in place remains in the swept region as trapped residual phase. In addition to the amount of trapped phase, its microscopic distribution within the pore space of a reservoir rock is important to gain a better understanding of recovery mechanisms and for the design and implementation of tertiary recovery processes. Despite the importance of the pore scale structure and distribution of residual oil, little quantitative information is currently available. We utilize a technique for imaging the pore-scale distribution of fluids in reservoir cores. The method allows the same core to be imaged after flooding under different wettability conditions, saturation states and flooding rates. Secondary and tertiary floods can be considered. Recovery mechanisms can be directly tested and the differences in the habitat of the residual fluids under different conditions can be directly quantified.

We present results for imbibition experiments on a number of sandstone and reservoir carbonate samples of varying complexity. The role of rate, wettability and initial water saturation on residual phase saturations are given. The detailed structure of the residual trapped phase is described; the size distributions of residual oil blobs, features of blob shape and dimensions are enumerated and compared under variable flooding conditions. These results provide an important platform for both the understanding of pore scale displacement mechanisms and for the testing and calibration of image and network-based models of multiphase flow.

INTRODUCTION

Unlike drainage, the physics and displacement mechanisms of waterflooding are non-trivial. A variety of conditions and mechanisms can affect waterflooding; these include variable wettability, displacement rates, brine compositions, the existence of films, the time dependent swelling of wetting films, the fluctuations in film pressure and thickness, and snap-off initiated cluster growth. Models that are currently developed to describe waterflooding processes rely on macroscopic observations of the displacement phenomenon, often observed on 2D glass micromodels of capillary ducts (Lenormand et al, 1983) with idealized fluids. Aside from these simple systems, there are very few other experimental processes that allow the observation of multiphase flow phenomenon. In this paper we undertake a number of waterflooding experiments of core samples and visualize the distribution of residual phase at the pore scale in three dimensions. We focus on the study of the trapped residual hydrocarbon saturation on

three important rock/fluid scenarios; as a function of the initial water saturation, the flooding rate and the wettability to oil and water (Morrow, 1987).

METHODS

Samples: The imbibition measurements were carried out on two Fontainebleau sandstone samples, two sucrosic dolomite samples and one reservoir carbonate exhibiting a more complex bimodal pore size distribution. All cores were of diameter 5 mm and lengths of at least 2 cm. The samples were imaged in three dimensions via μ-CT (Sakellariou et al., 2003) away from the ends of the core to minimize any end effects.

Experimental Methods: Spontaneous imbibition (SI) under strongly water-wet conditions was undertaken via the following methods: 1) Plasma clean core (Kumar et al, 2008); 2) Heat shrink the core with a carbon fibre rod attached at one end; 3) Overnight in vacuum oven at 60-70°; 4) Plasma clean the core again for 15 minutes; 5) Saturate under vacuum with 0.25M CsI-H_20 (μ=1cP, γ_{gw}=72mN/m) 6) Centrifuge in non-wetting phase to desired water saturation; 7) Seal off and allow core to equilibrate; 8) Bring core in contact with wetting phase reservoir. On completion of SI, seal core. 9) Image on μ-CT facility.

In another set of experiments we consider forced imbibition (FI) into the core after SI; in these cases 2 additional steps are undertaken. After imaging step 9, the sample is attached to a motor controlled syringe. The motor provides a constant driving force to drive CsI-H_20 into the sample. ~7-10 pore volumes of brine is injected through the system at varying capillary number. After this, we again image on μ-CT facility.

A final set of experiments is undertaken to investigate the role of wettability on the distribution of residual hydrocarbon (γ_{ow}=40mN/m). A technique for designing water wet (WW) and mixed wet (MW) cores was developed in the lab using (a) plasma cleaning and centrifugal drainage in air; (b) rapid freezing of the wetting phase to mask off certain pores in the sample using pre-prepared nitrogen slush, which is kept at a constant temperature of -230$^{\circ}C$; and (c) chemical masking of the remaining available pores, creating oil-wet surfaces. For the carbonate samples described here, steric-acid in heptane has been used.

The application of image registration (Latham et al, 2008) has made it possible to superpose, at voxel resolution, images of the same core volumes at different saturation states. Alignment of images is undertaken regardless of the elapsed time or the nature of the intervening experiment. This allows direct imaging of the fluid distribution in the pore-spaces of the same core in 3D under a range of wettability and saturation states. For all experiments described here, the total 3D image volume is 2000^3 voxels.

Methods for determination of magnitude, structure and habitat of Residual Phase: Several analyses were performed on the residual air/hydrocarbon blob structures identified in each imaging experiment. A first step is direct visual inspection of the habitat of the residual fluid in 3D; this provides a qualitative picture of the pore structures where hydrocarbon traps and gives information on the capillary structures of the residual phase. An example of a slice from a 3D image showing the residual oil after

waterflooding by SI is given in Fig. 1(a). Quantitative analysis is undertaken on the trapped clusters of residual phase; hereafter referred to as blobs. In a typical image over 2000 individual blobs are identified; a range of structural details can be provided on these blobs individually and collectively. Here we report the blob size distribution. Due to the irregularity of shape for such structures, description of blob size is not straightforward; we use an equivalent pore diameter based on the blob volume (d_{bv}). The full blob size distribution of all trapped residual phase clusters is given for each sample. Further quantitative analyses of the blob structure (e.g., interfacial area between wetting and non-wetting phase, curvature at phase boundaries, lineal extension, shape) can be quantified; due to space restrictions these are not described here.

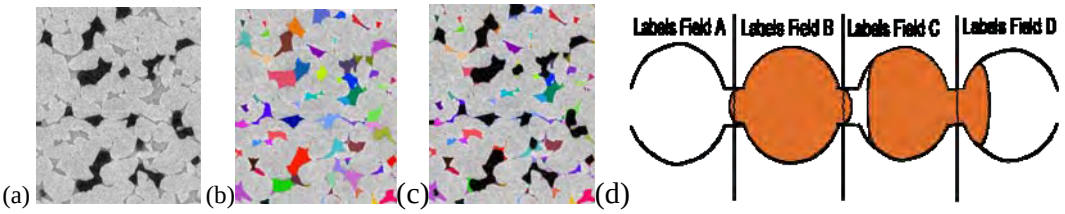

Figure 1: *Explanation of the labeling methodology used to describe the residual phase. (a) Slice of 3D image after spontaneous imbibition; trapped oil is black, water phase is lighter grey; (b) pore partitioning of the original pore space and (c) non-wetting phase distribution overlayed on the pore partition. (d) Schematic representation of the method for defining residual fluid occupancy. In label field A, the pore is filled by <10% non-wetting phase and in label field B-D, the gas phase resides in >10% of the pore space.*

Chatzis et al., 1988, described the shapes and unit sizes of pores in the context of the pore partitioning of the rock; sub-singlet, singlet, doublet, multiple and branched. For example, singlet blobs occupy one pore body and have sizes equivalent to a single pore. This analysis is undertaken on the image data presented here. A partitioning algorithm is used to define the boundary of each pore and the occupancy of pores defined for each isolated blob of non wetting phase. Fig. 1(b) shows the pore partitioning (Sheppard et al, 2005) of the slice in (a) and (c) shows an overlay of the blobs within the pore partitioning. One can observe that many of the blobs extend over a number of pores within one 2D slice. The definition of pore occupancy is illustrated in Fig. 1(d) where the residual phase is given by the shaded blobs. An ambiguity in pore occupancy arises in scenarios when a blob partially fills a pore. We define a pore as occupied by the residual fluid if the pore contains more than 10% of that fluid. For example, in Fig 1(d), the blob in pore field B is a singlet as it covers more than 10% of the pore in field B but less than 10% of the pore in field A and C. The blob in field C is a doublet as it covers more than 10% of the pores in both field C and D. The choice of 10% is somewhat arbitrary, however we have also undertaken analyses with other occupation definitions (e.g. 50% occupancy) and the overall trend of the blob size distributions is not affected by the choice of occupancy.

Hence, the overall algorithm used to define the residual phase is: 1) Wet image registration onto dry image; 2) Pore partitioning of the dry image. 3) Identification of all residual non-wetting blobs or ganglia. 4) Overlaying these 2 partitioned files to determine the size distributions and unit sizes of the residual non-wetting phase.

RESULTS

Effect of Initial Water on Residual (Gas) Saturations

A sequence of experiments was undertaken on 2 different Fontainebleau cores; one with $\phi \sim 19.7\%$, permeability (κ) ~ 3000 mD and a second with $\phi \sim 13.5\%$, $\kappa \sim 1800$ mD; ϕ data is obtained from MICP on sister subsample and κ via measures on original plugs. In this section, we image the resultant gas phase distribution (S_{gr}) after spontaneous imbibition into the core at varying S_{wi}. Results of the experiments are summarized in Table 1.

Sample	ϕ_{image} (%)	S_{wi}^{exp} (%)	S_{gr}^{image} (%)	$S_{gr}^{Suzanne}$ (%)	N_b^{med}, d_{bv}^{med} (μm)	N_b^{max}, d_{bv}^{max} (μm), S_b^{max} (%)
1-1	18.6	0	28.9	~30	9-10/ 250	142/ 880/ 7
2-1	14.1	0	41.7	~50	9-10/ 250	597/ 1160/ 11
2-2	14.1	30	45.9	~50	13-14/ 290	731/ 1180/ 10
2-3*	14.1	30	49.8	~50	12-13/ 250	284/ 990 / 9
2-4	14.1	60	15.2	~25	16-17/ 380	98/ 590/ 25

Table 1. *The image porosity (ϕ_{image}) is obtained from segmentation of the dry image of the imaged core material. SI experiments are undertaken at various initial water saturations (S_{wi}^{exp}). Saturations of the residual gas phase measured from the image (S_{gr}^{image}) are also given. Also given in the table is extracted data from Suzanne et al, 2003, for the residual gas ($S_{gr}^{Suzanne}$) for samples with similar ϕ:κ at the S_{wi} investigated here. N_b^{med} and d_{bv}^{med} represent the median unit size and equivalent pore diameter respectively. Also given in the last column is the maximum N_b and d_{bv} in the system, along with the % of the entire pore space this largest blob occupies (S_b^{max}).*

Fontainebleau Sandstone: Sample 1: $\phi \sim 19.7\%$; $\kappa \sim 3000$ mD

Fig. 2(a) shows a (2000 x 2000 pixel) slice through the 3D image of the clean sandstone in a dry state and Fig. 2(b) the same slice of the core after undertaking a SI experiment into the dry core under strongly water-wet conditions. The distribution of the residual gas can be directly visualized in 3D. In Fig. 2(c) we show a small 3D visualization of a subset of the core and the distribution of the water and residual gas. In (b) and (c) we observe that the non-wetting (gas) phase is trapped in the larger pores and the water is in the smaller throats and forms films around the larger pores. The residual gas saturation is measured on the image data via segmentation of the fluid in the pore regions. The value is estimated from the image as S_{gr} =28.9%. Data from Suzanne et al, 2003 for a similar sample ($\phi \sim 18\%$, $\kappa \sim 3850$ mD) measured a S_{gr}~30%. This is in agreement with the image based result.

(a) 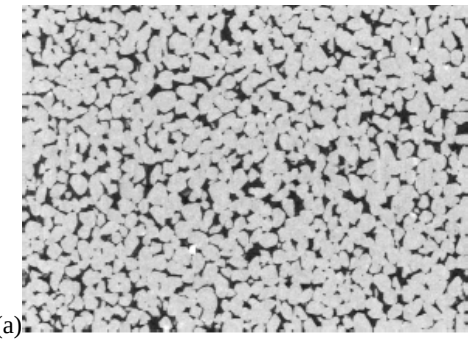 (b) 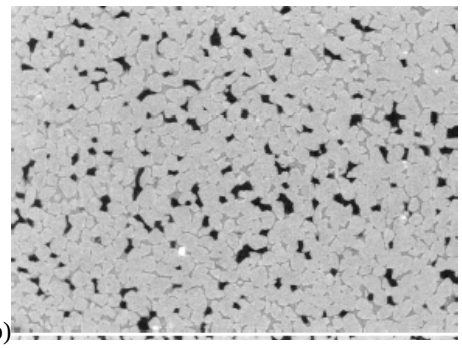

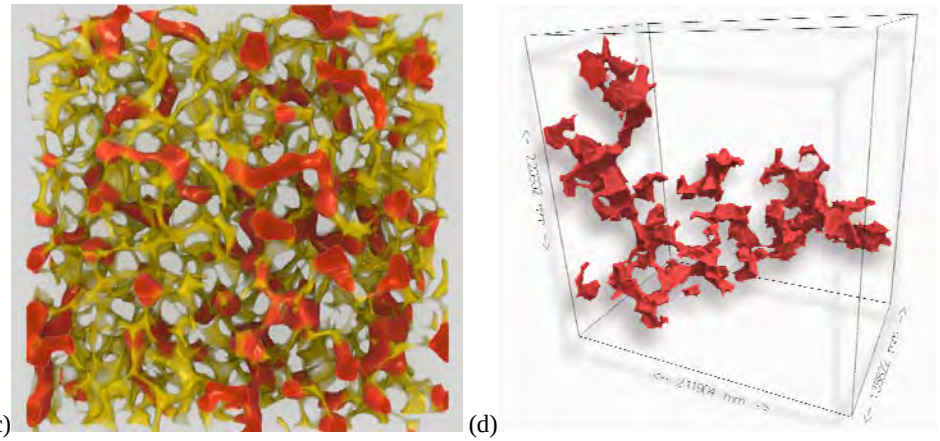

(c) (d)

Figure 2: *(a) Slice of Fontainebleau sample dry, ϕ_{image}~18.6%; (b) after SI into a dry system. (c) 3D visualization of a small subset of the 3D volume at residual gas saturation; the yellow shows the pore structure of a 1.8x1.8x0.5mm subvolume of the full image and red the trapped gas phase. (d) shows a 3D rendered image of a single large residual blob; the blob spans 104 pores (voxel resolution ~3.1 μm) and volume ~0.143 mm^3. The spatial extent of the blob is ~2x2x1 mm.The volume shown is <3% of the total image volume (6mm)^3.*

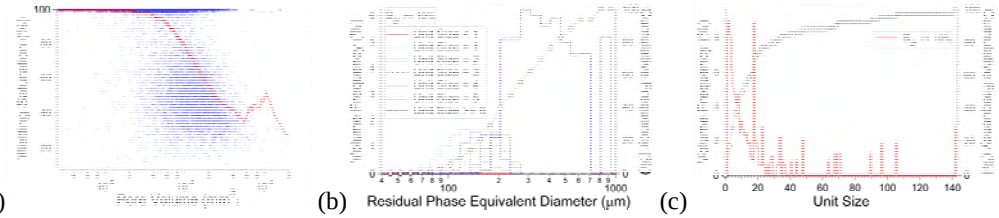

(a) (b) (c)

Figure 3: *(a) Scatter plot (blue points) displaying the wetting saturations of the 28000 individual pores. The red line gives the running average of the saturation across the pore sizes; (b) The residual blob size distribution as a function of unit size. Most trapped clusters reside across many pores. (c) The contribution to the residual saturation from blobs of different unit size.*

Gas Blob Characterization

In this experiment we identify 28,000 pores and 69,000 throats in the image volume and observe 1821 individual trapped blobs of residual gas. Fig 3(a) shows the distribution of the gas phase as a function of pore volume. As observed visually, the data shows a strong correlation between pore size and wetting phase saturation. The intermediate to large pores have low water saturations with the higher water saturations concentrated in the smallest pores. Fig. 3(b) describes the sizes of the residual gas blobs. The size distribution on a volume weighted basis for sub-singlets, singlets, doublets etc. through blobs of pore occupancy of 6 or greater is shown. The distribution of residual blobs is dominated by regions with larger N_b. The median d_{bv} is ~250 μm. N_b as a function of the total residual volume is shown in Fig. 3(c). We find the median N_b in pore units spanning >9 pores. Blobs that span multiple pore lengths may be considered likely targets for EOR (Chatzis et al., 1988). An illustration of a large trapped residual gas blob from this sample is shown in Fig. 2(d). This trapped cluster spans > 100 pores, is extremely ramified and is seen to extend over several pore lengths. The percentage of the trapped phase associated with the largest trapped cluster (S_b^{max}) in this sample is S_b^{max} = 7% .

Fontainebleau Sandstone: Sample 2: $\phi \sim 13.5\%$; $\kappa \sim 1800$ mD

Given that the imaging method employed is non-destructive one can perform multiple experiments on the same pore architecture. We visualize and quantify the difference in the residual fluid distributions in 3D after performing 5 experiments on sample 2 at different S_{wi}'s of 0%, 30% (x2), 40% and 60%.

Repeatability of Experiment: Given the small sample size and the fast imbibition rates (< 1 min) into the small samples we test whether the water saturation observed in 3D can be duplicated across multiple experiments. To test this we undertake two SI experiments on the same sample initially drained to S_{wi}=30%. Visual inspection of Fig. 4(a-b) shows that the pore-scale distribution of the water phase is spatially similar in the two experiments. The residual gas saturation is similar for the two samples (S_{gr} =46% & 50%).

S_{gr} vs. S_{wi}: Fig. 4(c) shows the same registered slice as in (a)/(b), though the 3D image of the clean sandstone after SI was performed at S_{wi}=0%. Very little difference in the distribution of the trapped saturation is observed. Fig. 4(d) shows the residual saturations measured for the samples compared to data from Suzanne et al, 2003 on a core with similar poro:perm ($\phi \sim 13\%$; $\kappa \sim 1660$ mD). The correlation to the available experimental data is satisfactory. The data points obtained in the above experiments match the piece-wise linear relationship between S_{gr} and S_{wi}, best described by Aissoui's law (Aissoui et al, 1983).

Gas Blob Characterization

The distribution of the residual gas blob sizes and the number of pores associated with each blob are shown in Fig. 5. A range of trends are observed. In the region where the residual gas saturation plateaus ($0\% < S_{wi} < 30\%$) there is little variation in the distribution of the trapped gas cluster size. This and the visual inspection of Figs. 4(a-c) indicates that both the residual saturation *and* the local pore scale distribution of trapped phases is invariant despite the different S_{wi}. The samples at S_{wi}>30% exhibit larger median blob sizes despite the residual being at significantly lower S_{gr}. Comparing Sample 1 and 2 at the same S_{wi} (=0%) we observe that the median blob size and unit size increases with decreasing porosity.

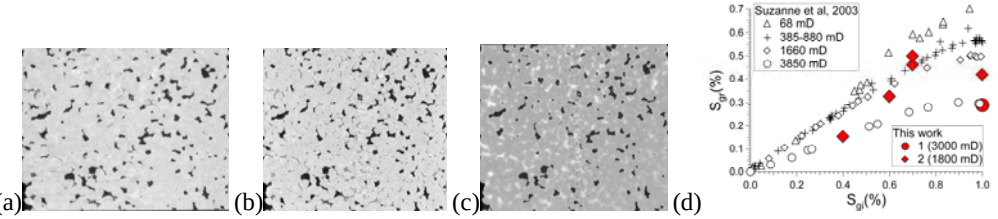

Figure 4: *(a) Fontainebleau sandstone after SI into a system with initial water saturation (S_{wi}) = 30% (b) SI into S_{wi} = 30% (repeat),(c) SI into S_{wi} = 0%, (d) Graph displaying data from Suzanne et al, 2003, with overlayed data from the above runs.*

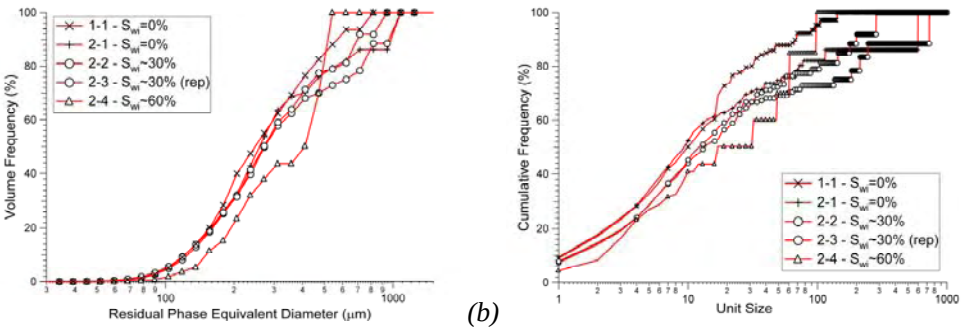

(a) *(b)*

Figure 5: *Distribution of (a) residual blob size and (b) unit blob size with different $S_{wi.}$ Data is shown for Sample 1 and Sample 2 at multiple saturations.*

Reservoir Carbonate: Experiments are performed on a reservoir carbonate sample with ϕ~23%; k~100mD; the sample exhibits a strong bimodal distribution of accessible pore throat sizes. Approximately 50% of the porosity is accessible via pore throats of radius, r_t>5 μm while the remainder accessible in the range r_t<1 μm. A subset of the slice within the 3D image is shown in Fig. 6(a). The total image volume is made up of 422,000 pores. Figs. 6 (b-d) illustrate the residual gas phase at S_{wi}=0%, S_{wi}~40% and ~50% respectively.

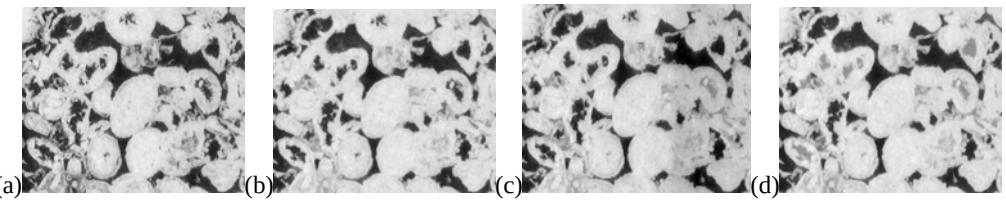

(a) (b) (c) (d)

Figure 6: *Subset of 3D μ-CT image of reservoir carbonate of size 1.35x1.05 mm in size (450 x 350 pixels, at 3 microns per pixel); (a) dry sample; (b) registered slice after SI at S_{wi}=0%; (c) registered slice after SI at S_{wi}~40%; (d) registered slice after SI at S_{wi}~50%.*

At S_{wi}=0%, we see gas trapped in the connected and the disconnected (moldic) macropores. In the situation where there is initial water, many of the moldic macropores are now water filled. Careful inspection of the images also reveals that more water is observed in the connected macropores during flooding at higher S_{wi}. However most of the residual phase lies in the connected macroporosity in all three samples. Details of the statistics of the residual saturations in the three different cases are given in Fig. 7 and Table 2. One observes that much of the residual is dominated by a few large clusters of trapped gas—indicating that the trapped gas may be associated with a percolation transition. In all three cases the largest trapped gas blob encompasses over 4000 pores (blob volume ~ 0.75 mm^3 for core of volume ~ 61 mm^3). We note that the size distribution of trapped gas decreases slightly with S_{wi}.

S_{wi}^{exp} (%)	ϕ_{image} (%)	S_{gr}^{image} (%)	N_b^{med}, d_{bv}^{med} (μm)	N_b^{max}, d_{bv}^{max} (μm), S_b^{max} (%)
0	24 (12)	47.9	91-92/ 250	5251/ 1190/ 20
40	24 (12)	37.8	27-28/ 190	4124/ 1110/ 10
50	24 (12)	38.2	51-52/ 220	5254/ 1130/ 25

Table 2. *Details of carbonate sample studied after SI. We report the total porosity after inclusion of the microporous fraction and the resolved porosity (given in brackets).*

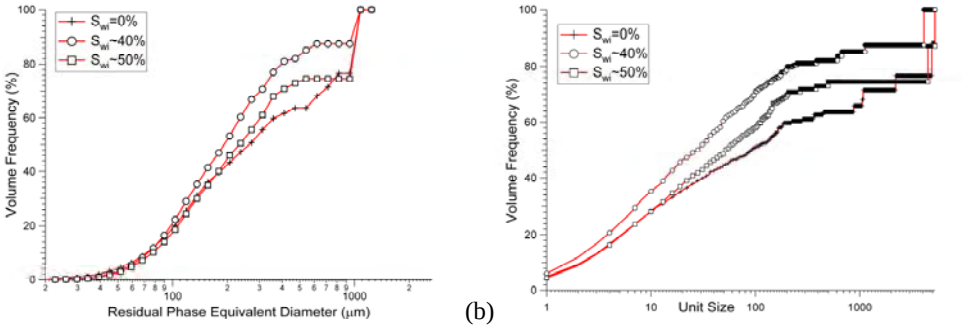

(a) (b)

Figure 7: *(a) Equivalent Diameter of the residual phase after drainage and SI on the bimodal carbonate sample; (b) Unit Size distribution. The larger trapped clusters at S_{wi}~50% compared to ~40% may be due to the presence of thicker films at the higher S_{wi} leading to enhanced snap-off.*

Effect of Rate on Residual (Oil) Saturations

It is well established that increased recovery can be obtained by immiscible displacement, if the capillary number (Ca) increases to beyond a certain critical value (Chatzis & Morrow, 1984). Using μ-CT we investigate rate effects on residual oil saturation, and in particular, the viscous force required for mobilization of a residual oil blob trapped under water wet conditions. For these experiments we consider a sucrosic dolomite core (ϕ=15%, k=900 mD) under very strongly water wet conditions. Registered slices through the 3D image of the sample after primary drainage to S_{wi}=31% are shown in Fig. 8(a) and in 8(b) after SI to a remaining oil saturation or S_{or} =37%. The sample was then flooded across a range of Ca until mobilization of the residual oil was observed. Consistent with data for Berea sandstone (Chatzis et al, 1983), mobilization occurred for Ca of the order of $2x10^{-4}$ (Fig. 8(c)) with the S_{or} after FI =28% (Amott Index = 0.8). In Fig. 9 we show a 3D visualization of the change in the residual oil structure after SI (Fig 9(a)) and after FI (Fig 9(b)) on the identical small 1.4 x 1.2 x 1.0 mm subset of the sample. We visually observe a lower trapped oil saturation and significant mobilization of the residual oil phase after FI.

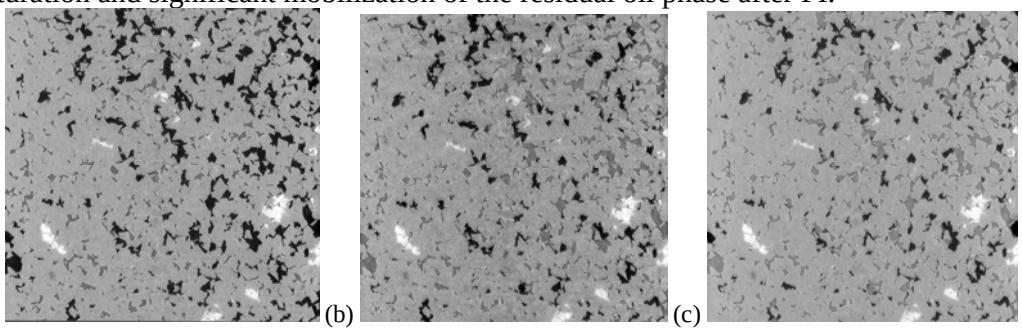

(a) (b) (c)

Figure 8: *Slice of 3D μ-CT image of sucrosic dolomite; (a) after drainage; (b) registered slice after SI; (c) after FI at Ca~$2x10^{-4}$; oil phase is black and water phase is the grey intermediate between oil and the dolomite matrix.*

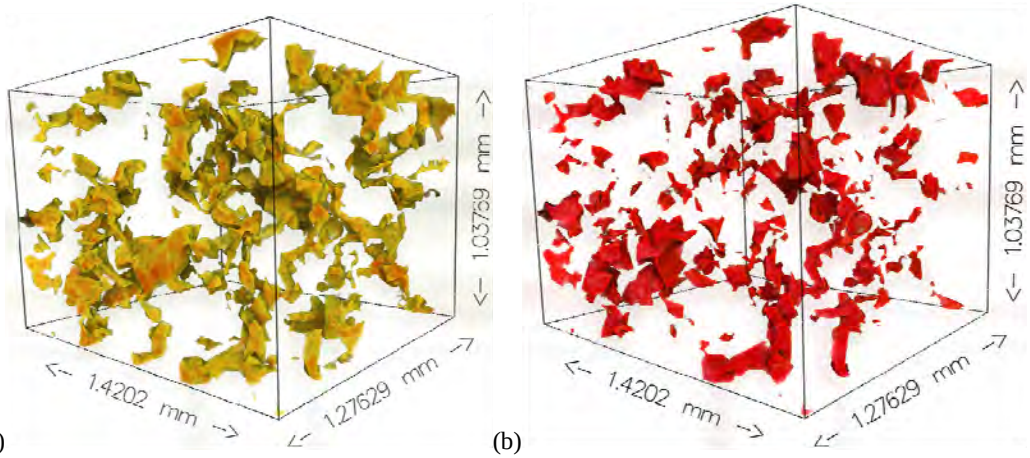

(a) (b)

Figure 9: *3D visualization of μ-CT image of sucrosic dolomite; (a) after SI; (b) after FI at Ca~2x10^{-4}. The residual oil phase is clearly observed as mobilized in (b).*

Blob Size Distribution: The distribution of the residual oil blob sizes and the number of pores associated with each blob are summarized in Fig. 10 and Table 3. As observed visually, N_b^{med} and d_{bv}^{med} decreases significantly with the mobilization of oil. As discussed by Chatzis et al, 1988, the viscous forces required for mobilization of a trapped oil blob is inversely proportional to length. The data shown in Fig. 10(a) indicates that mobilization is occurring in the larger trapped clusters while the blob size distribution for blobs of equivalent diameter (<100 μm) is consistent. The median and maximum blob size also decreases significantly after mobilization (Table 3).

State	S_{or}^{image} (%)	N_b^{med}, d_{bv}^{med} (μm)	N_b^{max}, d_{bv}^{max} (μm), S_b^{max} (%)
Drainage	69		
SI	37	15-16/ 192	366/ 690/ 8
FI: Ca~10^{-4}	28	8-9/ 180	114/ 520/ 9

Table 3. *Data for runs into strongly water wet sample after SI and FI.*

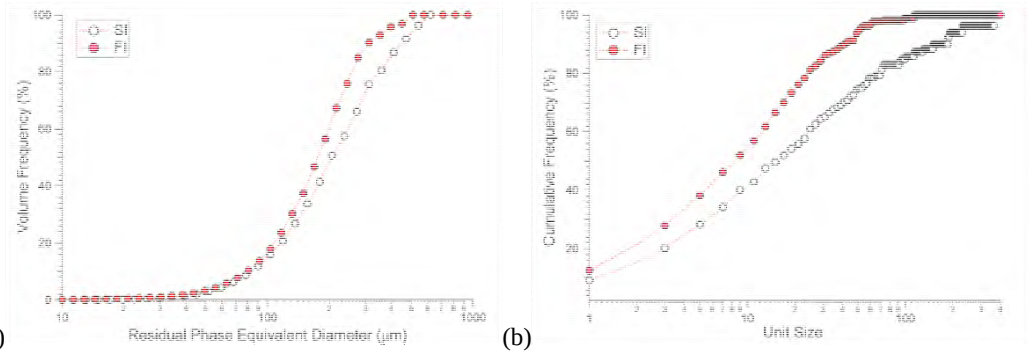

(a) (b)

Figure 10: *(a) Equivalent Diameter of the residual phase after SI and FI; Note that the larger clusters have been mobilized after FI while the smaller clusters remain. (b) Unit Size distribution.*

Effect of Wettability on Residual (Oil) Saturations

Wettability has an important impact on waterflooding processes. However reservoir wettability estimation and restoration remain controversial subjects; wettability changes due to the presence of crude oil are extremely complex. In this section we generate model mixed wet dolomite cores via a chemical treatment; steric-acid in heptane.

Three samples are considered; a very strongly water wet system (VSWW), described in Fig. 8-10, and two samples with lesser degrees of water wettability. The two samples are exposed to steric acid with a remaining water saturation of 75% and 30% respectively. We define these samples as WW and MW respectively. Although Amott tests were not undertaken on the samples we would expect that the samples exhibit decreasing values of the wettability index, $I_{w\text{-}o}$. Images of the WW and MW samples after SI (S_{wi} ~ 32%) and FI are given in Fig. 11 and results for the distributions of residual fluids detailed in Table 4 and Fig. 12. The main conclusions one can make from this initial study are:

1. While similar saturations are observed after flooding, the distribution of the trapped oil is visually different. In particular, the median and maximum residual blob size increases significantly after SI into the more mixed wet state. This larger blob size could be associated with a lowering of the effective coordination number of the pathways accessible to waterflooding under spontaneous conditions.
2. In all cases oil is mobilized after flooding at $Ca>5x10^{-5}$. The distribution of the blob sizes is very similar after FI in all three cases; little wettability effect is noted.
3. In FI, there is significant breaking up of the residual blobs. Larger blobs are broken up as observed by Chatzis, 1988. The median and maximum unit size and blob size decreases significantly in all cases. In the experiments after FI the wettability alteration does affect the local distribution of fluids; however the residual fluid seems to reside in similar blob sizes.

In these systems we note that S_{or} (WW) > S_{or} (VSWW) after FI, which is counter to the prevailing view in the literature (e.g., Salathiel, 1973, Fleury, 1999). However experiments in literature were undertaken under mixed or intermediate wet conditions and/or performed after ageing in crude oil. In many cases improved recovery was noted after the injection of significant numbers of pore volumes. The investigation of these and other important questions associated with flooding of mixed wet systems form a significant part of our ongoing research.

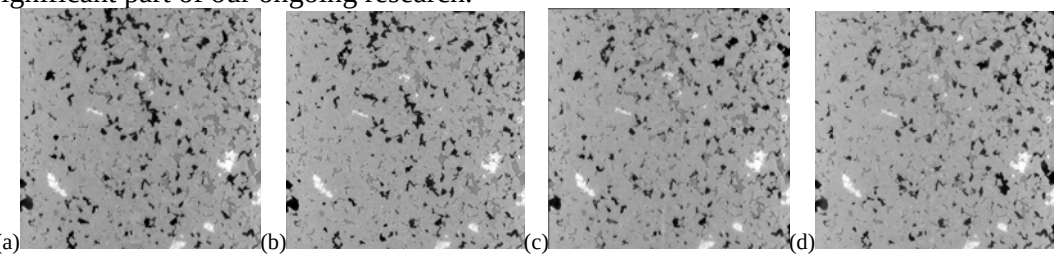

Figure 11: *(a) WW sample after SI, S_{or} ~ 35.9% compared to (b) MW sample after SI, S_{or} ~ 42.1%. (c) WW sample after FI. The S_{or} is ~ 31.9% compared to (d) MW after FI; S_{or} is ~ 34.6%.*

State	S_{or}^{image} (%)	N_b^{med}, d_{bv}^{med} (μm)	N_b^{max}, d_{bv}^{max} (μm), S_b^{max} (%)
VSWW - SI	36.9	15-16/ 192	366/ 690/ 8
VSWW – FI~10^{-4}	28.6	8-9/ 180	114/ 520/ 9
WW – SI	35.9	33-34/ 291	1768/ 1180/ 10
WW – FI~10^{-4}	31.9	7-8/ 180	127/ 560/ 7
MW – SI	42.1	54-55/ 337	4314/ 1600/ 20
MW – FI~10^{-4}	34.6	8-9/ 192	195/ 640/ 8

Table 4. *Comparison of systems at different wettability.*

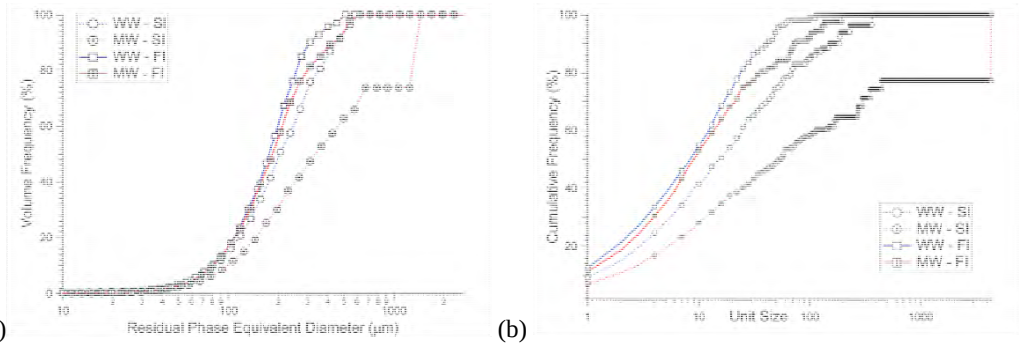

(a) (b)

Figure 12: *(a) Residual blob diameter and (b) unit size after SI and FI under different wettability conditions.*

CONCLUSIONS

- We present results for imbibition experiments on a number of sandstone and reservoir carbonate samples of varying complexity. The role of rate, wettability and initial water saturation on residual phase saturations are enumerated at the pore scale. In all cases studied large residual blobs (spanning from 100 to thousands of pores) were observed after waterflooding via SI or FI.
- The trapped residual saturation was measured at the pore scale as a function of initial water. Data for Fontainebleau sandstone is in agreement with data from Suzanne et al., 2003 and consistent with the empirical relationship of Aissoui, 1983.
- The effect of displacement rate on residual saturation follows the results of Chatzis and Morrow, 1984; for a water wet sample we find ROS decreasing with increased capillary number. We also observe a similar rate effect in mixed wet core. The mobilization of the trapped phase is observed for $Ca > 5 \times 10^{-5}$.
- Initial studies show pore scale changes in ROS after SI under model mixed wet conditions. In particular, the median and maximum residual blob size increases significantly. Differences are less noticeable after FI at higher rates.

ACKNOWLEDGEMENTS

The authors thank member companies of the Digital Core Consortium for funding support and the Australian Partnership for Advanced Computation for computing resources.

REFERENCES

1. Aissoui, A., 1983, Etude Théorique et Expérimentale de l'Hystérésis des Pressions Capillaires et des Perméabilités Relatives en Vue du Stockage Souterrain de Gaz, Thesis Ecole des Mines de Paris (1983), 223 p.
2. Chatzis, I., Morrow, N. R., and Lim, H. T., 1983, Magnitude and Detailed Structure of Residual Oil. Society of Petroleum Engineers Journal, **23**, 311 – 330.
3. Chatzis, I. and Morrow, N. R., 1984, Correlation of Capillary number Relationships for Sandstone. Society of Petroleum Engineers Journal, **24**, 555 –562.
4. Chatzis, I.; Kuntamukkula, M. S. & Morrow, N. R., 1988, Effect of Capillary Number on the Microstructure of Residual Oil in Strongly Water-Wet Sandstones, Society Of Petroleum Engineers Reservoir Engineering, **3**, 902 - 912

5. Fleury, M., Branlard, P., Lenormand, R., and Zarcone, C., 1999, Intermediate wettability by chemical treatment. Journal of Petroleum Science and Engineering, **24**, 123 – 130.
6. Kumar, M., Senden, T.J., Latham S., Sheppard, A.P., Knackstedt, M.A., Cinar, Y., and Pinczewski V.W., 2008, Designing for Mixed Wettability, Society of Petroleum Engineers, **Paper No. 113862**, 1 – 12
7. Latham, S.; Varslot, T. & Sheppard, A. P., 2008, Image Registration: Enhancing and Calibrating X-ray Micro-CT Imaging, Society of Core Analysts, **Paper No. 35**, 1 - 12
8. Lenormand, R., Zarcone, C., and Sarr, A., 1983, Mechanisms of the displacement of one fluid by another in a network of capillary ducts. Journal of Fluid Mechanics, **135**, 337 – 353.
9. Morrow, N.R.: "A Review of the Effects of Initial Saturation, Pore Structure, and Wettability on Oil Recovery by Waterflooding," *Proc.* North Sea Oil and Gas Reservoirs, Trondheim (Dec. 2-4, 1985) Graham and Trotman, Ltd., London, 1987, 179-91.
10. Salathiel, R. A., 1973, Oil recovery by surface film drainage in mixed wettability rocks. Journal of Petroleum Technology, **25**, 1216 – 1224.
11. Sakellariou, A.; Sawkins, T. J.; Senden, T. J. & Limaye, A., 2003, X-Ray Tomography for Mesoscale Physics Applications Physica A, **339**, 152 - 158.
12. Sheppard, A. P., Sok, R. M., and Averdunk, H., 2005, Improved Pore Network Extraction Methods, Society of Core Analysts, **Paper No. 20**, 1 – 12.
13. Suzanne, K., Hamon, G., Billiotte, J., and Trocme, V., 2003, Experimental relationships between residual gas saturation and initial gas saturation in heterogeneous sandstone reservoirs. Society of Petroleum Engineers, **Paper No 84038**, 1 – 12